Available online at www.sciencedirect.com

SciVerse ScienceDirect

Ceramics International 39 (2013) 4269–4279

CERAMICS INTERNATIONAL

www.elsevier.com/locate/ceramint

Effect of high energy milling on the formation and properties of sialon ceramics prepared from silicon nitride-aluminium nitride precursors

Malgorzata Sopicka-Lizer[a,*], Cihangir Duran[b], Hasan Gocmez[c], Tomasz Pawlik[a], Marta Mikuskiewicz[a], Ken MacKenzie[d]

[a]*Silesian University of Technology, Faculty of Materials Engineering and Metallurgy, Katowice, Poland*
[b]*Department of Materials Science and Engineering, Gebze Institute of Technology, Gebze-Kocaeli, Turkey*
[c]*Department of Ceramics Engineering, Dumlupınar University, Kutahya, Turkey*
[d]*MacDiarmid Institute for Advanced Materials and Nanotechnology, School of Chemical and Physical Sciences, Victoria University of Wellington, New Zealand*

Received 18 June 2012; received in revised form 4 October 2012; accepted 5 November 2012
Available online 16 November 2012

Abstract

Nanostructured silicon nitride and aluminium nitride powder mixtures have been successfully produced by high-energy mechanical activation. Subsequent high sintering activity and β-sialon formation at low temperature resulted from activation milling at high acceleration. Densification of the samples prepared from the activated powders commenced at temperatures by about 200 °C lower, as compared with the samples prepared from the non-activated powder mixture. ^{27}Al MAS NMR spectra clearly showed the effect of mechanical activation on the structural changes and phase evolution of the sialon precursor during heat treatment. After pressureless sintering at 1600 °C for 60 min, β-sialon samples had a Young's modulus of 281 GPa, microhardness of 12.8 GPa, fracture toughness of 4.6 MPa $m^{0.5}$ and flexural strength of 632 ± 129 MPa. The unique structure and bi-modal grain size distribution that is retained after conventional sintering at 1600 °C opens up new possibilities for tailoring the microstructure and related properties of these materials.

Keywords: A. High-energy milling; A. Powders: solid state reactions; A. Sintering; D. Si_3N_4

1. Introduction

If mechanical milling is used in a traditional sense, the process does not produce a new material since the microstructure of the powder particles does not change. Mechanochemical processing (or mechanical activation), on the other hand, involves structural changes accompanying the simultaneous particle size reduction. Thus, this process includes mechanical milling, mechanical alloying and reaction milling, during which particle deformation, fracture and welding processes occur due to the ball/powder collisions. The resultant structural changes determine the reactivity of the activated powder and both the specific surface area and elastic strain energy are increased. However, the response of the material depends on its mechanical properties and crystal structure. The acquired energy can be relaxed by the fracture of brittle material, by polymorphic transformations resulting from crystal lattice rearrangement, or by mechanochemical decomposition/synthesis (the formation of new chemical compounds). On the other hand, the elastic strain energy can transform into plastic energy of lattice defects (vacancies, dislocations, subcrystallite interfaces) and structural disorder [1]. The occurrence and kinetic of these processes depends on the stressing conditions and an amount of energy introduced during high-energy milling.

Mechanical activation is important in many applications such as waste processing and production of advanced materials with enhanced microstructures and properties. Moreover, a top–down method of mechanochemical processing has the advantage of relative simplicity and availability. A particle obtained by means of high energy milling differs from a particle of the same size obtained by a bottom–up synthesis method, because mechanical activation of the powders results

*Corresponding author. Tel.: +48 32 6034476; fax: +48 32 603 4400.
E-mail address: malgorzata.sopicka-lizer@polsl.pl (M. Sopicka-Lizer).

0272-8842/$ - see front matter © 2012 Elsevier Ltd and Techna Group S.r.l. All rights reserved.
http://dx.doi.org/10.1016/j.ceramint.2012.11.006

in lower sintering temperatures and higher densities required for many applications. Also, mechanochemical synthesis of mixed oxides with ionic bonds is well known [2–4]. The availability of new planetary mills with higher acceleration and higher energy densities has facilitated mechanical activation of more covalently bonded compounds with higher lattice energy such as mullite [5], quartz [6] or SiC [7]. Recent papers show that mechanochemical activation can be successfully applied to sialon precursors [8–13] and highly defective nanostructured particles can be obtained [12]. If a β-Si_3N_4-based precursor with AlN and alumina additives is mechanically activated for 4 h, then full densification by spark plasma sintering is reported to be possible at 1550 °C for 5 min [10]. However, these papers do not differentiate between the role of mechanical activation of the sialon precursor and the fast spark plasma sintering on the densification and β-sialon precipitation. In order to further explore the mechanical activation of the advanced ceramic powders and their ability for nanoceramic formation, their susceptibility to deformation under high-energy planetary milling must be examined because pressureless sintering to obtain nanostructured Si_3N_4-based ceramics would have advantages for industrial applications over spark plasma sintering under a pressure of 30 MPa. Besides, reduction of densification temperature and elimination of pressure sintering of Si_3N_4-based ceramics by variety of means were the goals of several studies [14–17]. Application of high-energy milling of the relevant precursor could be the prospective solution for pressureless densification of nitride ceramics and mass production of the components for the wear resistant application.

Alternatively, several attempts have been made to produce silicon nitride or β-sialon nanostructured ceramics from nanosized powders [18–21]. The results clearly showed that the previous knowledge about the microstructure control of silicon nitride ceramics must be updated, as the high sintering activity of the nanopowders allows the processes of densification and adjustment of the microstructure to be separated [20–21]. Moreover, nanosized β-Si_3N_4 crystallites/nuclei embedded in amorphous oxynitride nanopowder favour the formation of a fine microstructure at lower sintering temperatures and enhance intensive anisotropic grain growth at higher temperatures [20]. Therefore, mechanical activation of β-Si_3N_4 particles opens new possibilities for tailoring the microstructure development of the resultant ceramics.

In this study, mechanochemical activation of Si_3N_4-based precursors using a new design of high energy mill with an acceleration up to 50G (G, gravitational acceleration) was studied. The effect of varying the gravitational acceleration (e.g., 0G, 28G and 50G) and the activation time (30 and 60 min) on the powder properties, densification behaviour and mechanical properties of the resultant ceramics were also investigated.

2. Experimental procedure

Sialon precursors were prepared for mechanochemical activation using α-Si_3N_4 (H.C. Starck-B7), β-Si_3N_4 (Aldrich, −325 mesh, containing traces of Si_2N_2O and α-Si_3N_4), AlN (H.C. Starck-C) and Y_2O_3 (H.C. Starck-C) powders. The Si/Al ratio was set to $z=0.4$ β-sialon solid solution composition. In addition, AlN was used instead of alumina in batch compositions to avoid oxygen excess in the system if oxidation occurred during activation milling. Two types of batch were prepared: α-Si_3N_4-based (A-type) and β-Si_3N_4-based (B-type). The batches contained 5 wt% of Y_2O_3 as sintering aid, however, one A-type batch (designated as A_0) was prepared without Y_2O_3. The precursors were prepared by mixing the respective powders with isopropanol on a roller bench for 24 h and then dried at 105 °C. The activation milling was performed in a new design of planetary mill (MPP-1, TTD Ltd. Russia) at accelerations of 28G for 30–60 min in air or at 50G for 30 min in argon atmosphere in a veil with silicon nitride lining and using silicon nitride balls. Precursor powder and the milling media were placed into the veil by keeping the ball-to-powder weight ratio at close to 7:1. Details of this process and the new planetary mill are described elsewhere [12]. Unmilled control samples, designated as A-RB (α-Si_3N_4-based) and B-RB (β-Si_3N_4-based), were derived from powders mixed on the roller bench. After activation or mixing, the powders were dispersed in an aezotropic mixture of methylethylketone + ethanol with a dispersing agent (hypermer KD1), ultrasonically homogenized for 1 h, mixed again on the roller bench for 24 h then dried at room temperature. Only one unmilled batch (A-RB) was not homogenized with addition of a dispersant. The applied procedure was necessary for deagglomeration of the milled powder. The specific surface areas of the activated and mixed powders were determined by the BET method (ASAP 2010) after deagglomeration. The powders were uniaxially pressed into 20 mm diameter tablets and then cold isostatically pressed at 250 MPa. The polymer binder was slowly burnt out by heating at 2 °C/min in air to 600 °C and holding at this temperature for 2 h. The samples were then placed in a BN crucible on a Si_3N_4/BN powder bed and densified in a graphite furnace (Thermal Technology) under flowing nitrogen (3 l/h) at 1200–1600 °C for 1 h. Dilatometry (SETARAM) and DTA/TG (NETZSCH) was carried out under both air and nitrogen atmospheres at 20–1600 °C with a heating rate of 10 °C/min. The mass and dimension changes after shaping and heating were also recorded. The densities of the sintered samples were determined by the Archimedes method.

The phase compositions and unit cell parameters of the activated powders and sintered pellets were determined from Rietveld refinement of XRD data obtained using a Philips-Panalytical X'pert-PRO system with a continuous step scan (0.0080° 2θ step size and 957.6 s scan time). The accuracy of the calculated lattice parameters was 0.0005 Å. The z-value of β-sialon solid solution was calculated according to the Ekström's formula [22]. The nitrogen and oxygen contents were measured by infrared analysis of CO produced by hot-gas extraction (ELTRA ON). The activated powders were examined using a Hitachi

Table 1
Phase composition (amorphous phase was not measured), specific surface area and oxygen content of the initial A and B mixtures as-batched and as-activated.

Precursor	Crystalline phase composition as-calculated from XRD, wt%					SSA, $m^2 g^{-1}$	Oxygen content, wt%
	α-Si_3N_4	β-Si_3N_4	AlN	Y_2O_3	Si_2N_2O		
A-initial (A-RB), unmilled	73	16	6	5	0	5.5	2.3
A-30 min-28G, air	81.6	14.4	3.2	0.8	0	18.7	3.9
A_0-initial, unmilled	77.1	16.9	6	0	0	5.4	1.2
A_0-30 min-28G, air	80.6	16.3	3.1	0	0	18.9	2.4
B-initial (B-RB), unmilled	4	80	6	5	5	5.5	3.6
B-30 min-50G, argon	0	96.3	0	0	3.7	27.9	5.84
B-60 min-28G, air	0	96.4	0	0	3.6	21.9	5.81

high resolution transmission electron microscope. ^{27}Al and ^{29}Si MAS NMR spectroscopy was carried out on powdered heat-treated samples at a field of 11.7 T using a Varian Unity 500 spectrometer with a 5 mm Doty MAS probe spun at 4 kHz for Si and a 4 mm Doty probe spun at 10–12 kHz for Al. The ^{27}Al spectra were acquired using a 1 μs ($\pi/10$) pulse with a 1 s recycle delay and are referenced to $Al(H_2O)_6^{3+}$. The ^{29}Si spectra were acquired using a 6 μs ($\pi/10$ pulse for solution) with a 100 s delay and are referenced to tetramethyl silane (TMS).

The specimen derived from 50G activated powder of the B-type and sintered at 1600 °C was chosen for TEM studies after cross-sectioning. The thin foils for transmission observations were cut out with Ga^+ focused ion beam (FIB) technique using QUANTA 200 3D system equipped with Omniprobe lift-out attachment. The polished specimen surface was covered with thin carbon coating to minimize the image drift during cutting out of the FIB specimen. The microstructure observations were performed using a TECNAI G^2 FEG 20 (200 kV) equipped with EDAX integrated X-ray Energy Dispersive Spectroscopy (EDS) microanalysis system. The scanning-transmission images were acquired using HAADF detector at 200 mm camera length. The electron diffractions patterns were taken at parallel illumination and using selected area diffraction aperture, i.e. Selected Area Diffraction Pattern (SADP) mode.

The Vickers hardness of the samples was determined at a load of 10 kg and the fracture toughness was calculated from the Palmquist cracks after the Vickers indentation using the Niihara approach [23]. The elastic modules were determined using a UZP-1 (INCO-VERITAS) ultrasonic tester. The ultrasonic wave velocity was measured in two perpendicular directions of the specimen diameter and along its height. The anisotropy of the elastic modulus and of the wave velocity was calculated as $A = 100^*(E_\perp - E_{||})/E_\perp$, where $E_\perp$, $E_{||}$ are the elastic modules in the perpendicular and parallel directions of uniaxial pressing, respectively. The flexural strengths were measured on $2 \times 5 \times 15$ mm cut and polished specimens using INSTRON equipment. Each test was made on 4–5 replicates. The fractured surface of those samples was observed in FE-SEM microscope (Philips XL-30) after sputtering with gold.

3. Results and discussion

3.1. Effect of activation on crystallinity and phase composition

Activation milling at high energy density gives rise to significant changes in particle properties even after very short milling times. The compositions of the batched and activated powder mixtures are presented in Table 1. The β-Si_3N_4 starting powder was found to be contaminated by both Si_2N_2O and α-Si_3N_4 (B-RB), while α-Si_3N_4 powder contained up to 16 wt% of β-phase (A-RB). Milling at 28G and 50G results in sialon precursor powders with specific surface areas that are increased over that of the starting powders by nearly four times and five times, respectively. XRD phase analysis shows that AlN and Y_2O_3 reflections broaden and eventually disappear after activation, suggesting that AlN and Y_2O_3 crystal lattices have been destroyed to such an extent that they do not produce well-defined diffraction lines. Thus, the results after activation milling, as-presented in Table 2, are affected by the presence of the amorphous phase(s) although they were not considered in composition calculations. Also note that the balls before and after milling were weighed out and mass losses below 0.1 wt% were recorded.

Silicon nitride is less susceptible to activation milling than the oxide components and AlN. The α/β-Si_3N_4 ratio varies slightly after milling but these changes can be ascribed to both amorphization and oxidation. The β-Si_3N_4 peaks are broader and less intense only in samples subjected to longer milling times or higher acceleration. Attempts to measure the mean crystallite size from the broadening of diffraction lines by Hall–Williamson method did not give reliable results, possibly because the observed line broadening originates from a variety of crystal lattice defects apart from the finite grain/crystallite size (Scherer's formula) and stress-induced broadening (Williamson's equation). Several structural crystal defects such as dislocations and plastic deformation were indeed observed by TEM in the β-Si_3N_4 particles (Fig. 1a and b) if compared with the HRTEM image of the unmilled particle (Fig. 1c). The HRTEM images show severe crystal lattice damages responsible for the reduced area of coherent scattering of the X-ray radiation after activation.

Table 2
Phase composition (wt%) of the B-RB, B-60 min-28G and B-30 min-50G after isothermal heat treatment at 1200–1600 °C. Accuracy of the measurement fell in the range of 0.2–0.4.

Phases in B-type specimens	Prior to heating	Temperature, °C				
		1200w	1300	1400	1500	1600
β-Si_3N_4						
B-RB	80	87.7	90.2	86	89.7	92.4
B-28G-air	96.4	90.6	88.5	89.3	91.9	90.8
B-50G-argon	96.3	91.5	93.9	97.8	100	100
Si_2N_2O						
B-RB	5	1.8	0	0	0	0
B-28G-air	3.6	7	9.6	10.7	8.1	9.2
B-50G-argon	3.7	3.3	1.5	0	0	0
α-Si_3N_4						
B-RB	4	3.6	0	4.1	1.3	0
B-28G-air	0	2.4	1.8	0	0	0
B-50G-argon	0	0	0	2.2	0	0
YAG						
B-RB	0	1.3	4.2	6.9	9	7.6
B-28G-air	0	0	0	0	0	0
B-50G-argon	0	0	0	0	0	0
AlN						
B-RB	6	5.7	5.6	3.1	0	0
B-28G-air	0	0	0	0	0	0
B-50G-argon	0	0	0	0	0	0
Al_2O_3						
B-50G-argon	0	5.2	4.5	0	0	0

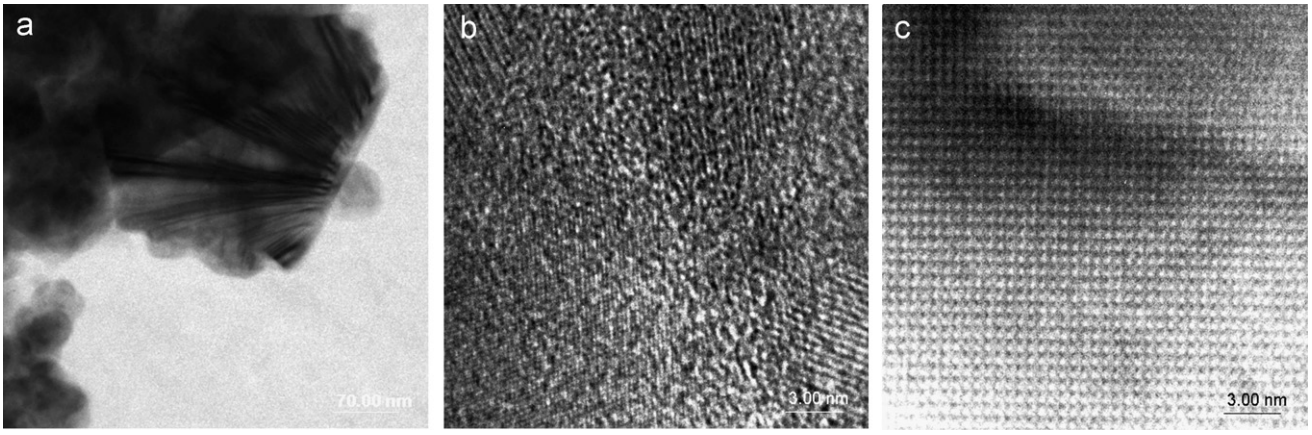

Fig. 1. TEM images of a β-Si_3N_4 particle: (a) after activation milling with 50G acceleration and (b) HRTEM image; and (c) HRTEM image of a non-milled silicon nitride particle.

The formation of structural defects also resulted in an increase of the unit cell volume of the silicon nitride. For example, it increased from 145.61×10^{-6} pm^3 at 0G to 145.71×10^{-6} pm^3 at 28G and to 145.73×10^{-6} pm^3 at 50G. Activation milling led to an increased oxygen content in the powders, but by replacing alumina with AlN and milling in an argon atmosphere (B-30 min-50G), the total oxygen content could be limited to a level expected in a β-sialon solid solution of $z=0.4$ with 5 wt% of Y_2O_3 (3.2 wt%) plus oxygen contamination in the initial powder (Table 1, A_0-initial unmilled powder). The oxygen content of the both activated samples B-60 min-28G (air) and B-30 min-50G (argon) were of the same order despite the higher surface area of the latter (see Table 1). Since the phase composition as measured by XRD remains the same for both specimens prior to heating (Table 2), it could be assumed that defective amorphous areas in the particles activated in argon retain more nitrogen showing the positive effect of milling in an inert atmosphere. In contrary, the oxygen rich amorphous spots/scales are then more susceptible to oxidation to silicon oxynitride at elevated temperature as evidenced by phase composition results (Table 2).

3.2. Effect of liquid phase and densification

The activated (milled) and deagglomerated powders show high compaction ability, resulting in green densities of about 2.00–2.07 g cm^{-3} (i.e., 62–64.1% of theoretical density based

Table 3
Densities and mass change of the specimens after heat treatment at 1500 °C and 1600 °C for 60 min+and − signs refer to mass gain and loss, respectively.

Precursor	Green density, g cm^{-3}	1500 °C		1600 °C	
		Sintered density, g cm^{-3}	Mass change, wt%	Sintered density, g cm^{-3}	Mass change, wt%
A-initial (A-RB), unmilled	1.61	1.98	+1.49	2.61	+2.89
A-30 min-28G, air	2.07	3.02	−0.33	3.11	−0.56
A_0-initial, unmilled	1.88	1.96	+1.81	2.16	+3.11
A_0-30 min-28G, air	2.01	2.35	+0.27	2.48	+0.20
B-initial (B-RB), unmilled	1.91	2.15	+1.62	2.79	+2.99
B-30 min-50G, argon	2.07	3.11	−1.51	3.20	−1.70
B-60 min-28G, air	2.00	3.10	−1.16	3.15	−1.50

on 3.23 g cm^{-3}), compared to about 1.88–1.91 g cm^{-3} (i.e., 58–59%) in the non-activated (unmilled) but deagglomerated samples (Table 3). The unmilled batch (A-RB) that was not homogenized with addition of a dispersant, was compacted to a green density of 1.61 g cm^{-3} (i.e., 50%). The linear shrinkage after isothermal sintering to almost full density for the samples with green density over 60% was found to be as low as 13%. Shrinkage rate curves given in Fig. 2 compare the effect of activation and presence of Y_2O_3 sintering additive on the pressureless densification behaviours of the A and A_0 samples. Densification of the samples prepared from the milled powders (A-30 and A_0-30) commenced at much lower temperature than the samples prepared from the unmilled powders (A_0-initial) by about 200 °C (~1050 °C versus ~1250 °C) as-estimated from the shrinkage rate curves. It should be noted that since the A_0 specimens did not contain yttria, a liquid phase was not expected in the eutectic temperature range (1350 °C) [24]. Therefore, the initial densification of the milled yttria-free samples must be related to the effect of particles rearrangement and/or softening of the amorphous Si–Al–O–N phase. Thus, start of densification by mean of particle rearrangement occurs at a temperature about 200 °C lower (A_0-30) in comparison with the non-activated one (A_0-initial) with the same composition, which is attributed to the effect of activation.

The consequence of the yttria addition and liquid phase formation in the activated samples becomes apparent if the shrinkage rate is compared between yttria-free (A_0-30) and yttria-containing specimens (A-30), both mechanochemically treated for the same time. Initially, the shrinkage rate for both specimens is the same for 1050–1150 °C range as we could expect for the particles sliding effect. Divergence between the two sintering rate curves occurs above 1150 °C; thus, the higher shrinkage rate of A-30 specimen above 1150 °C must be related to the formation of yttria-containing liquid phase and/or its lower viscosity. Consequently, it is assumed that eutectic liquid formation is lowered to that temperature as an effect of powders amorphization. However, parallel shrinkage rate curves over 1300–1400 °C show the quantitative effect of the temperature related amount and/or viscosity of the liquid phase as densification without yttria was moved to higher temperature.

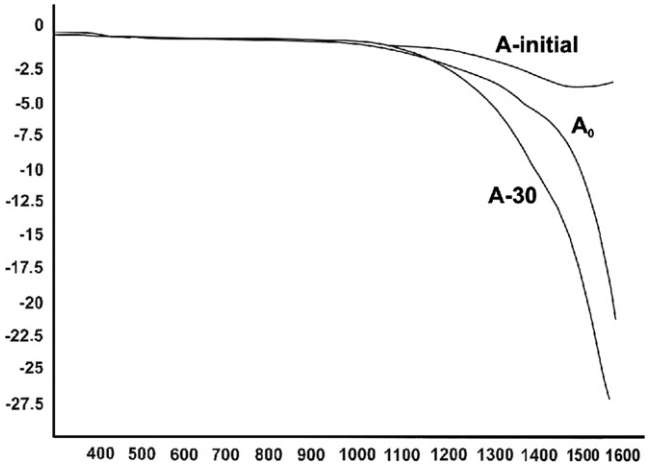

Fig. 2. Shrinkage rate curves of the unmilled A_0-initial, A_0-30 min-28G (A_0-30), and A-30 min-28G (A-30) under nitrogen flow.

The similar behaviour was observed for the activated B-based specimens as an increase of density was noticed after isothermal treatment of the compacted specimens above 1200 °C (Fig. 3). Fig. 3 also compares the densification behaviours of the A- and B-based samples. Samples prepared from unmilled B-type powders (B-RB) achieved 84.1 % relative density at 1600 °C, but samples prepared from activated powders were fully dense at 1600 °C, reaching 98.4% relative density (at 28G) and 99.8% (at 50G). This full degree of densification after activation under both conditions is consistent with the same oxygen content in both specimens (Table 1). However, it should be noted that the applied powder-bed environment for sintering was not sufficient to prevent mass transport in the gas phase since some mass gain was observed during consolidation of the non-activated precursors if they were heat-treated over 1400 °C (Table 3). In contrary, mass losses continued with raising temperature for the activated samples.

3.3. Mechanism of phase formation

The DTA plot of the B-30 min-50G sample shows an exothermic peak above 1325 °C under a nitrogen atmosphere (Fig. 4). This energy release can be attributed to the

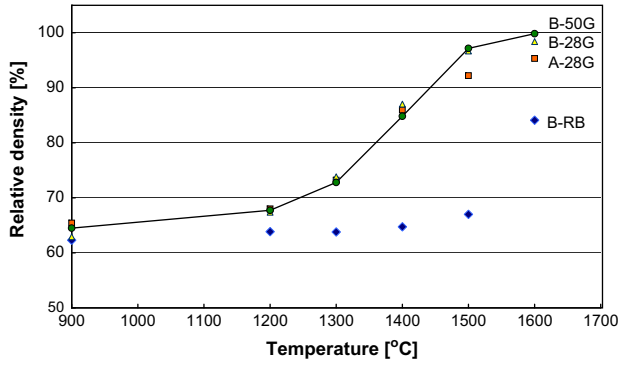

Fig. 3. The effect of the activation milling on densification of the B-type mixture.

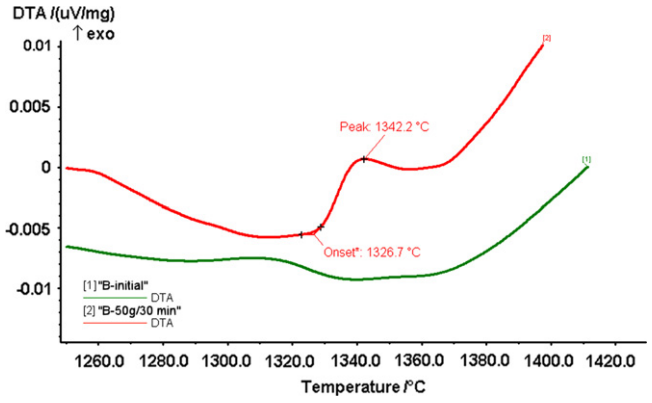

Fig. 4. DTA of the unmilled and activated with 50G B-type batches in nitrogen flow.

partial ordering/crystallization of the defective/amorphous Si–Al–Y–O–N phase.

The evolution of the phase composition in the β-Si_3N_4–AlN–Y_2O_3 activated powders was studied by calculating the phase compositions from Rietveld refinements of the XRD data (Table 2) and comparing them with the qualitative NMR results. β-sialon formation in the heat treated specimens was monitored by the measurement of the β-Si_3N_4 unit cell parameters (Fig. 5). Phase evolution is considerably influenced by the precursor activation history. The greatest activation effect (judged on the basis of the specific surface area reached in the B-30 min-50G sample) and milling in argon environment produced crystallization of α-Al_2O_3 after isothermal heat treatment at 1200 °C (see Table 2) and was followed by its dissolution in the eutectic liquid. Consequently, the small exothermic peak in Fig. 4 could be ascribed to crystallization of the amorphous Si–Al–Y–O–N phase to α-Al_2O_3. β-sialon was the only phase present in the specimens after heat treatment above 1400 °C (Table 2, $z=0.1$–0.3). It is interesting to note that formation of β-sialon solid solutions and the degree of substitution in the specimens derived from the activated powders began after isothermal heating at 1300 °C and increased smoothly in conjunction with the dissolution of alumina. The final z-value was close to 0.3, slightly lower than the targeted value of 0.4. Changes in the unit cell parameters (Fig. 5)

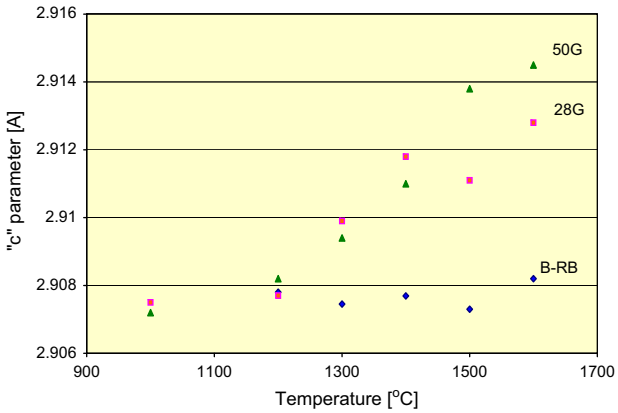

Fig. 5. The effect of activation on the β-Si_3N_4 lattice parameters in the B-based mixture as a function of sintering temperature.

mirror the densification behaviour shown in Fig. 3; thus, increase of β-sialon solid solution was related to the properties of the liquid phase as confirmed by TEM/EDS studies (Fig. 6). The small rounded grains containing only silicon and nitrogen (area no. 3) are embedded in the Si–O–N–Al–(Y) phase (area no. 2) while the greater ones are enriched with Al and O thus their chemical composition is typical of β-sialon.

In contrast, activation at 28G in air (B-60 min-28G) and subsequent heat treatment produced intermediate silicon oxynitride. The noteworthy presence of Si_2N_2O in the reacted specimens at higher temperature occurred only in the B-type specimens activated in air and the reason of that behaviour is not clear. It could be related to the presence of Si_2N_2O in the initial powder and/or to the oxygen specific position in nanoparticles since formation of Si_2N_2O was previously reported for nanopowder-derived silicon nitride ceramics [25]. Besides, the limited formation of O'-sialon as a result of reaction between the oxidized Al coatings on Si_3N_4 grains was reported after pressureless sintering of β-sialon at lower temperature [16]. It should be underlined that increase of z-value was stopped at 1400 °C as if the liquid phase did not contain a sufficient amount of nitrogen.

In contrary, the reference specimen (B-RB) was contaminated by YAG (Table 2). It thus appears that a crucial role in the phase development is played not by the total oxygen content but by the selective oxidation during activation milling. An oxygen deficiency in the non-activated reference specimen limited the dissolution of silicon and aluminium nitrides in the liquid up to 1500 °C or 1400 °C, respectively. As a result the formation of YAG was observed after heat treatment above 1200 °C but no β-sialon was detected as no change was observed in the β-Si_3N_4 unit cell parameters after sintering the non-activated precursor at 1200–1500 °C (Fig. 5). All suggest that subsequent oxide bearing phase development during heat treatment is coupled to both: activation milling in air and preliminary presence of Si_2N_2O.

More detailed information on the structural changes after heat treatment can be derived from the NMR studies. The identical ^{29}Si chemical shifts previously reported for

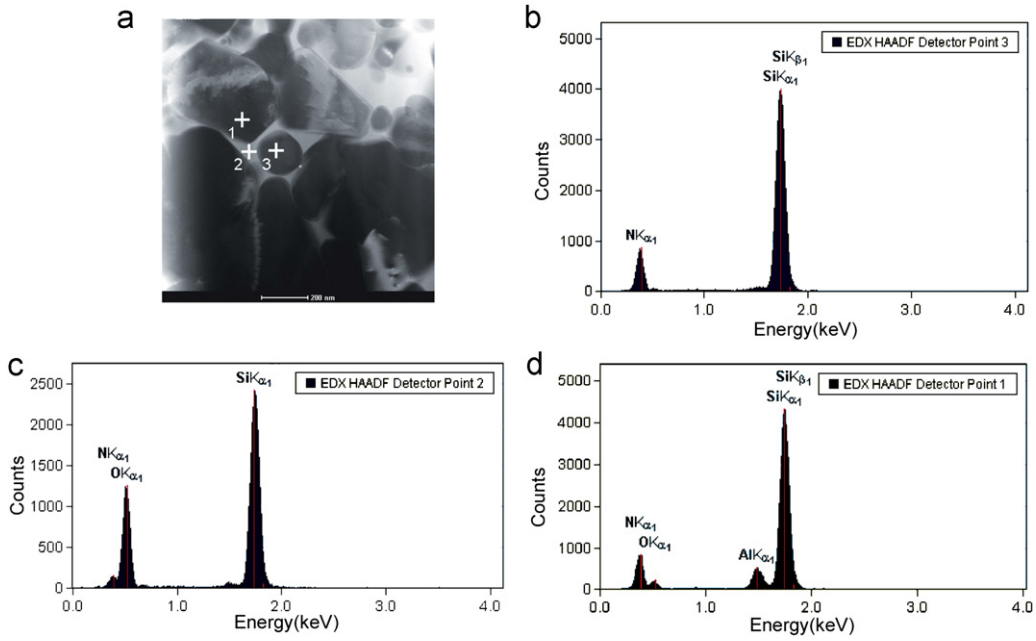

Fig. 6. HAADF-type scanning-transmission image of the B-30min-50G specimen after sintering at 1600°C for 60 min with points of EDS (a), EDS spectra were taken from a small grain (b), intergranular phase (c) and a large grain (d).

β-Si_3N_4 and β-sialon (−48.5 ppm) [26] make it impossible to distinguish between these phases by NMR, but the presence of Si_2N_2O (for example, as detected by XRD in sample B-50G) is confirmed in the ^{29}Si spectrum of this sample (not shown) by a small peak at −62 ppm [26]. There is little evidence in the ^{29}Si MAS NMR spectra of any of the samples in the presence of SiO_2, which has its characteristic NMR signature at about −110 ppm [26]. However, the ^{27}Al spectra (Fig. 7) reveal more subtle differences between the B-based unactivated and activated precursors heated to different temperatures since the range of Al-containing phases present have clearly distinguishable Al MAS NMR spectra. The spectrum of the expected product, β-sialon, is essentially independent of the *z*-value, and contains resonances at about 103 and 66 ppm, corresponding to tetrahedral AlN_4 and AlO_4 units, respectively [26]. The tetrahedral Al–O resonance at 66 ppm is broad and is probably composed of overlapping bands from a range of Al–O–N environments [26]. The unit giving rise to the Al–N resonance probably contains at least one oxygen nearest the neighbour since pure AlN has its peak at about 114 ppm [26]. The sialons often contain a small octahedral AlO_6 resonance at about 0 ppm that is not expected from the structure and is usually ascribed to impurity phases. The other Al-containing phases known to occur in the present samples have characteristic NMR resonances (α-Al_2O_3 at 13 ppm and YAG at 0.7 ppm) [26].

Based on these peak assignments, at the lowest heating temperature (1200 °C) the unmilled sample (Fig. 7b) shows a large amount of unreacted AlN (114 ppm) together with the formation of some β-sialon (a broad unresolved feature at 56–69 ppm) and YAG (0.8 ppm). Increasing the heating temperature results in a progressive increase in the β-sialon and YAG resonances, with the tetrahedral Al–O and Al–O–N units becoming progressively better resolved at 1400 °C, and the AlN peak at 114 ppm being replaced by the β-sialon peak at 103 ppm by 1600 °C. The progressive increase in the amount of YAG formation in the unmilled samples with increasing temperature is consistent with the XRD data, the structural changes in these samples suggesting the formation of a liquid phase after isothermal treatment at >1400 °C but with limited crystallization of β-sialon.

The ^{27}Al MAS NMR spectra of the milled precursors show significant structural changes on heating even at lower temperatures as compared with the unmilled specimens. At 1200 °C, more β-sialon has formed (evidenced by the broad unresolved feature at 57 ppm and the small feature at 105 ppm, Fig. 7d) in contrast to the unmilled sample given in Fig. 7b. A significant amount of α-Al_2O_3 is present (13 ppm) but the absence of a peak at 114 ppm indicates that most of the original AlN has been lost. On heating to higher temperatures, the broad tetrahedral β-sialon feature corresponding to a range of Al–O–N species becomes more pronounced and the intensity of the α-Al_2O_3 peak decreases, finally disappearing at 1500 °C. In the milled sample heated at 1600 °C (Fig. 7c), the dominant Al NMR feature is the broad, unresolved tetrahedral Al–O–N resonance centred at 59 ppm, with a minor β-sialon peak at 105 ppm also visible.

These experiments show that activation milling significantly reduces temperature of the eutectic liquid formation and enhances densification but the phase & microstructure development is related to the genuine effects of activation as well as the oxygen partial pressure during milling. AlN

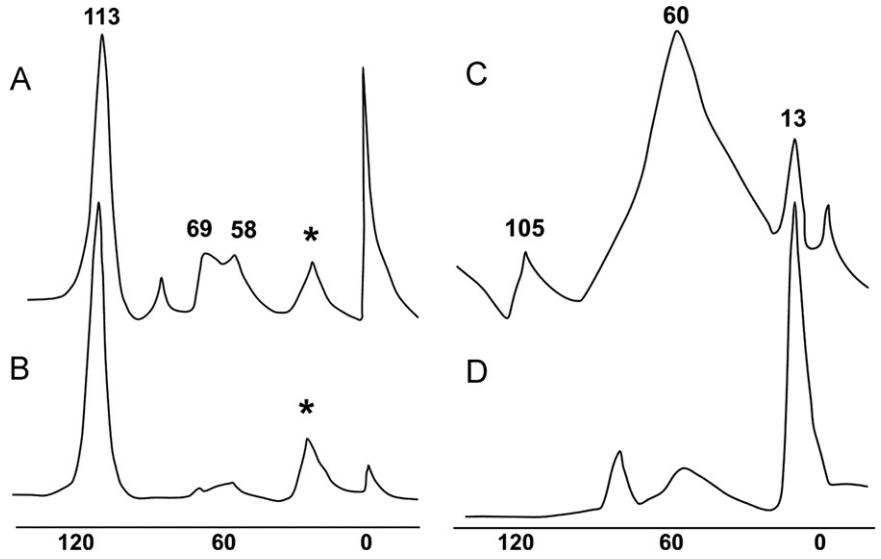

Fig. 7. A selection of representative 11.7T solid state ^{27}Al MAS NMR spectra of the B-based sialon precursor (unmilled and activated at 50G) after heat treatment: unmilled and heated at 1400 °C (a) and 1200 °C (b); activated and heated at 1600 °C (c) and 1200 °C (d). Asteriks denote spinning side bands.

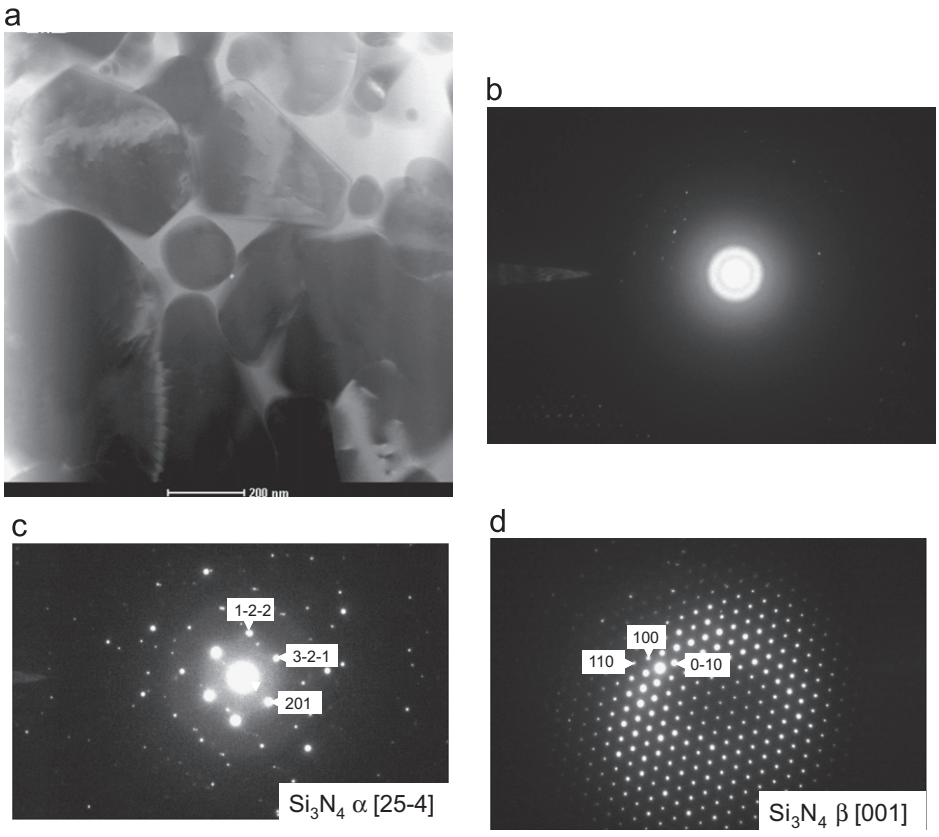

Fig. 8. HAADF-type scanning-transmission image of the B-30 min, 50G specimen (a) with the relevant electron diffraction patterns at the pocket of intergranular phase (b), small grain (c) and large grain (d) evidencing dissolution of small α-Si_3N_4 grains into surrounding yttria rich amorphous phase (light colour related to the greater atomic mass of elements).

in the tested system is the less resistant phase to oxidation and jointly with yttria deform under milling conditions. Mechanical milling promotes diffusion and atomic transfer during high-energy collisions of particles [29]; consequently they form a homogenous amorphous Al–Y–Si–(O,N) phase which favours the formation of the transient liquid phase at lower temperature by 200 °C during the subsequent heat treatment. Milling in air accelerates silicon nitride oxidation to the given extend (limited amount of oxygen in the closed jar) apart from AlN oxidation. Consequently, the nitrogen content in the ensuing defective-amorphous Al–Y–Si–(O,N) phase will depend on the oxygen partial

pressure during milling and it will govern the subsequent solution-precipitation process.

Milling in air the B-based composition produced crystallization of Si_2N_2O after heat treatment in nitrogen. The relevant data for the precursor milled at 28G in air demonstrate increase of the z value of β-sialon up to 0.1 in powders heat treated up to 1400 °C and insignificant increase to $z=0.18$ if the powder was annealed at 1600 °C. It means that the resultant liquid phase accelerated densification at temperature over 1200 °C (Fig. 3) but was deprived of nitrogen as it happens during densification of silicon nitride ceramics with alumina and yttria additives [27]. Since only α-Si_3N_4 could dissolve in the eutectic liquid at temperature below 1400 °C and to serve as a source of nitrogen and silicon, we assume that this phase was partially oxidized to Si_2N_2O during activation milling in air.

Alternatively, the very low oxygen partial pressure, as it occurred during milling in the argon atmosphere, resulted only in the limited oxidation and formation Al–Si–Y–O–N amorphous species with higher nitrogen content. Silicon nitride remained non-oxidized as evidenced by the lack of free silica in the ^{29}Si NMR spectrum. TG studies in air of B-30 min-50G sample (not shown here) evidence mass gain over 800 °C which can be ascribed to the oxidation of amorphous Al–Si–Y–O–N derived particles. In contrary, heating in nitrogen atmosphere must lead to ordering and crystallization of α-Al_2O_3 inside Al–Y–O–N amorphous species as this phase was detected by XRD and NMR after isothermal heating at 1200 °C. Determination of the unit cell parameters from the XRD data (Fig. 5) indicates the formation of a β-sialon solid solution upon heating the powder milled at 50G to > 1200 °C. The defective α-Si_3N_4 particles were susceptible to the eutectic liquid formation with amorphous or partially crystallized Al–Y–O matter at 1200 °C; Fig. 8 shows that small and large grains belong to α-Si_3N_4 (Fig. 8c) and β-Si_3N_4 (Fig. 8d) phases, respectively. Increase of temperature leads to further dissolution of small silicon nitride grains and subsequent growth of β-sialon solid solution.

3.4. Microstructure evolution and mechanical properties

It is generally accepted that the growth of β-sialon grains generally occurs via a transient liquid phase through the solution–diffusion–reprecipitation mechanism. Since the amorphous phase in the activated powders is far from

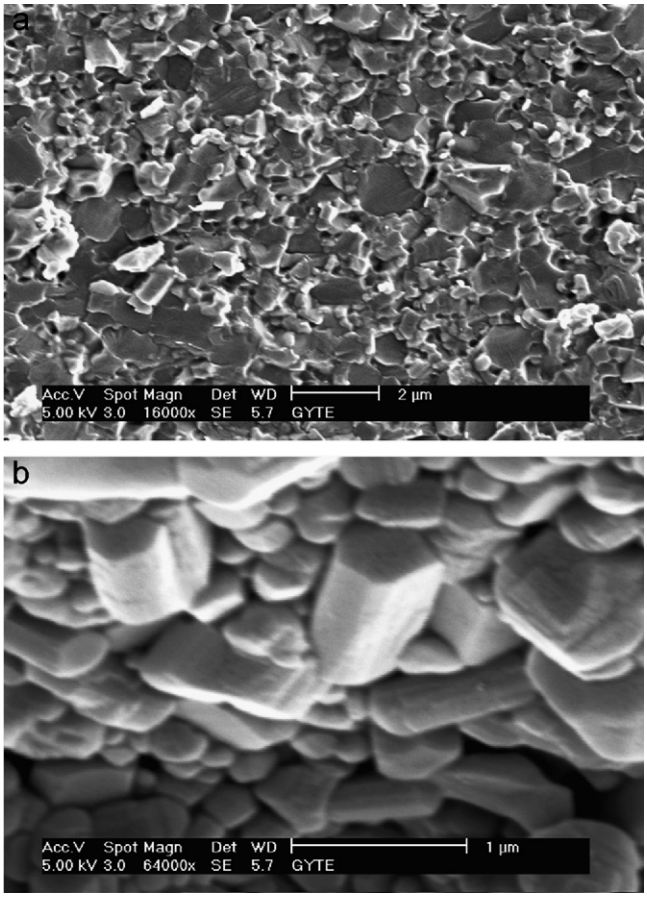

Fig. 9. Field emission scanning electron microscopy images of the fracture surface of the B-30 min, 50G specimen after sintering at 1600 °C showing bimodal distribution of the grain size and limited number of the elongated grains.

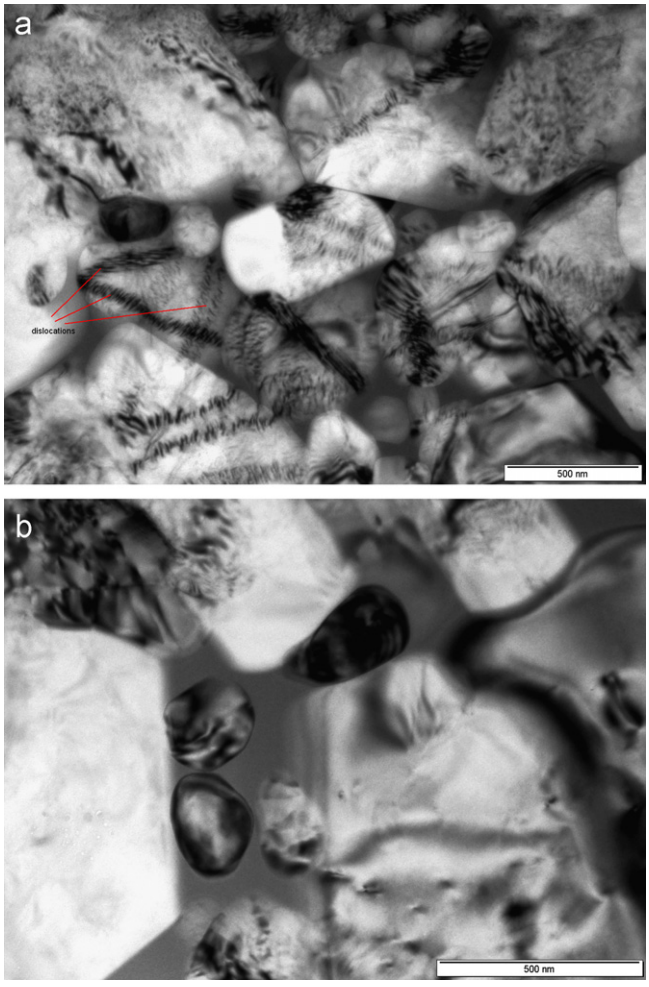

Fig. 10. TEM images of the B-30 min, 50G specimen demonstrating ordered dislocations in the greater β-sialon grains and the role of the small nanosized (below 200 nm) grains in strengthening the material.

Table 4
Mechanical properties of β-sialon samples after pressureless sintering at 1600 °C for 60 min.

Code	Young modulus, [GPa]	Microhardness, [GPa]	K_{1c},[MPa $m^{0.5}$]	Flexural strength, [MPa]
A-30 min-28G, air	234 ± 13	10.9 ± 0.3	5.72 ± 0.2	340 ± 29
B-60 min-28G, air	255 ± 13	13.7 ± 0.3	4.74 ± 0.2	400 ± 81
B-30 min-50G, argon	281 ± 8	12.8 ± 0.3	4.59 ± 0.2	632 ± 129

the thermodynamic equilibrium, the formation of β-sialon must occur via growth of the large number of the existing β-Si_3N_4 grains assisted by aluminium and oxygen transport via liquid phase. Thermal treatment of the B-based specimens induces grain growth in primary β-Si_3N_4 phase and a solid solution formation by diffusional transfer of matter through an oxynitride liquid phase, evidenced by a small but particularly well resolved ^{29}Si NMR resonance at −62 ppm in the B-30 min-50G samples heated at 1200 °C and 1300 °C (not shown here). Due to the high viscosity of liquid at these relatively low temperatures, dissolution of silicon nitride and grain growth of the primary β-Si_3N_4 grains is suppressed, resulting in low anisotropy of the microstructure and bi-modal grain size distribution (Fig. 9). The average diameter of the β-Si_3N_4 grains varies in the range of 0.5–2 μm and most of the grains are equiaxed with sharp crystal habit, indicating a typical growth by diffusional matter transfer through a liquid. DTA studies did not show any significant energy release during heat treatment over 1300 °C; thus, relaxation of the acquired energy during activation milling must have happened by slow dislocation ordering accompanied by mass transport. TEM micrographs show well-ordered dislocations and thin grain boundaries between some grains (Fig. 10a). Relatively low sintering temperature allowed full densification of β-sialon ceramics but dissolution of α-Si_3N_4 particles was not completed after heat treatment at 1600 °C. The residual particles have round shape (effect of dissolution) with diameters below 200 nm and are embedded in the left-behind glassy phase (Fig. 10b). The resultant bi-modal distribution of the grain size and high isotropy of the microstructure formed after heating at 1500–1600 °C opens up the prospect of new possibilities for tailoring physical properties.

The mechanical properties of the samples sintered at 1600 °C for 60 min show that the present materials compare well with standard β-sialon ceramics (Table 4). The measured microhardness values fall in the range of typical hot-pressed β-sialon ceramics [28]. As the resultant microstructures (Fig. 9) are far from typical microstructure with elongated β-sialon grains having high aspect ratio, it can be assumed that small silicon nitride grains with diameter below 300 nm placed among the greater ones (Fig. 10b) must be responsible for comparable mechanical properties. The flexural strengths of the specimens derived from the precursors activated at 28G in air are lower than for typical β-sialon ceramics. On the other hand, the B-30 min-50G specimens containing a unique bi-modal microstructure show excellent mechanical properties such as Young's modulus of 281 GPa, microhardness of 12.8 GPa, fracture toughness of 4.6 MPa $m^{0.5}$ and flexural strength of 632 ± 129 MPa, which can be tailored to suit particular applications even though they are sintered under pressureless conditions at 1600 °C for 60 min.

4. Conclusions

Nanostructured silicon and aluminium nitride mixtures with and without Y_2O_3 additions have been produced by high-energy planetary milling. XRD patterns showed that activation significantly changed the initial materials in that the AlN and Y_2O_3 diffraction peaks became very broad or disappeared completely after long milling times. β-Si_3N_4 peaks, however, decreased in intensity and broadened only after the longest milling time or highest milling acceleration. Activation milling under high acceleration conditions in argon produced precursors which formed β-sialon at lower temperatures than in the unmilled mixtures, and proved to be readily sinterable. Densification of the samples prepared from the milled powders commenced at much lower temperatures by about 200 °C lower, as compared with samples prepared from the unmilled mixture. Densification and β-sialon crystallization occurred via a dissolution–precipitation mechanism supported by the solid state diffusion and was related to the extent of amorphization of the precursor. ^{29}Si and ^{27}Al MAS NMR spectroscopy clearly showed the effect of mechanical activation on the structural changes and phase development in the sialon precursors during heat treatment. Oxidation during high-energy milling strongly affects AlN particles and controls subsequent phase and microstructure evolution. β-sialon ceramics produced from a precursor milled at 50G for 30 min by pressureless sintering at 1600 °C for 60 min had a Young's modulus of 281 GPa, microhardness of 12.8 GPa, fracture toughness of 4.6 MPa $m^{0.5}$ and flexural strength of 632 ± 129 MPa. The resultant microstructure after densification at 1600 °C opens up new possibilities for tailoring the microstructure and related mechanical properties of these materials.

Acknowledgement

Financial support by the 6th FP under the project No. ACTIVATION NMP2-CT-2004-505885 and by Polish Ministry of Science under the project No. N507 373335 is gratefully acknowledged. The authors are greatly indebt

to dr hab. Jerzy Morgiel and dr Kinga Rodak for help in TEM studies.

References

[1] I.J. Lin, Implications of fine grinding in mineral processing mechanochemical approach, Journal of Thermal Analysis 52 (1998) 453–461.
[2] C.C. Koch, Synthesis of nanostructured materials by mechanical milling, Problems and opportunities 9 (1997) 13–22Nanostructured Materials 9 (1997) 13–22.
[3] J. Kano, S. Saeki, F. Saito, M. Tanjo, S. Yamazaki, Application of dry grinding to reduction in transformation temperature of aluminum hydroxides, International Journal of Mineral Processing 60 (2000) 91–100.
[4] E. Kostic, S. Kiss, S. Boskovic, Decrease of the $MgAl_2O_4$ formation temperature, Powder Technology 92 (1997) 271–274.
[5] J. Temuujin, K. Okada, K.J.D. MacKenzie, Formation of mullite from mechanochemically activated oxides, The Journal of the European Ceramic Society 18 (1998) 831–835.
[6] H. Heegn, F. Birkeneder, A. Kamptner, Mechanical activation of precursors for nanocrystalline materials, Crystal Research and Technology 38 (2003) 7–20.
[7] D. Chaira, B.K. Mishra, S. Sangal, Synthesis and characterization of silicon carbide by reaction milling in a dual-drive planetary mill, Material Science & Engineering A (2007) 111–120.
[8] K.J.D. MacKenzie, J. Temuujin, M.E. Smith, K. Okada, Y. Kameshima, Mechanochemical processing of sialon compositions, Journal of the European Ceramic Society 23 (2003) 1069–1082.
[9] K.J.D. MacKenzie, D.V. Barneveld, Carbothermal synthesis of β-sialon from mechanochemically activated precursors, Journal of the European Ceramic Society 26 (2006) 209–215.
[10] X. Xu, T. Nishimura, N. Hirosaki, R.-J. Xie, Y. Zhu, Y. Yamamoto, H. Tanaka, New strategies for preparing nanosized silicon nitride ceramics, Journal of the American Ceramic Society 88 (2005) 934–937.
[11] X. Xu, T. Nishimura, N. Hirosaki, R.-J. Xie, Y. Yamamoto, H. Tanaka, Fabrication of β-sialon nanoceramics by high-energy mechanical milling and spark plasma sintering, Nanotechnology 16 (2005) 1569–1573.
[12] M. Sopicka-Lizer, M. Tańcula, T. Włodek, K. Rodak, M. Hüller, V. Kochnev, E. Fokina, K.J.D. MacKenzie, The effect of mechanical activation on the properties of β-sialon precursors, Journal of the European Ceramic Society 28 (2008) 279–288.
[13] T. Nishimura, X. Xu, K. Kimoto, N. Hirosaki, H. Tanaka, Fabrication of silicon nitride nanoceramics—Powder preparation and sintering: a review, Science and Technology of Advanced Material 8 (2007) 635–643.
[14] G. Ling, H. Yang, Pressureless sintering of silicon nitride with magnesia and yttria, Materials Chemistry and Physics 90 (2005) 31–34.
[15] Z. Tatli, D.P. Thompson, Low temperature densification of silicon nitride materials, The Journal of the European Ceramic Society 27 (2007) 791–795.
[16] C. Zhang, R. Janssen, N. Claussen, Pressureless sintering of β-sialon with improved green strength by using metallic Al powder, Materials Letters 57 (2003) 3352–3356.
[17] C.R. Zhou, Z.B. Yu, V.D. Krstic, Pressureless sintered self-reinforced Y-α-SiAlON ceramics, The Journal of the European Ceramic Society 27 (2007) 437–443.
[18] F.I. Bulić, I. Zalite, N. Zhilinska, Comparison of plasma-chemical sythesized SiAlON nanopowder and conventional prepared SiAlON powder, Journal of the European Ceramic Society 24 (2004) 3303–3308.
[19] A. Bellosi, J. Vicens, V. Medri, S. Guicciardi, Nanosize silicon nitride: characteristic of doped powders and of the related sintered materials, Applied Physics A 81 (2005) 1045–1052.
[20] M. Herrmann, I. Schultz, I. Zalite, Materials based on nanosized β-Si_3N_4 composite powders, Journal of the European Ceramic Society 24 (2004) 3327–3335.
[21] M. Herrmann, Z. Schen, I. Schultz, J. Hu, B. Janear, Silicon nitride nanoceramics densified by dynamic grain sliding, Journal of Materials Research 25 (12) (2010) 2354–2361.
[22] T. Ekström, P.O. Kall, M. Nygren, P.O. Olsson, Dense single-phase β-sialon ceramics by glass-encapsulated hot isostatic pressing, Journal of Materials Science 24 (1989) 1853–1861.
[23] K. Niihara, A fracture mechanics analysis of indentation-induced Palmquist crack in ceramics, Journal of Materials Science 2 (5) (1983) 221–223.
[24] I.A. Bondar, F.Ya. Galakhov, Izvestiya Akademii Nauk SSSR, Seriya Khimicheskaia 7 (1964) 1325–1326.
[25] J.-H. Kim, B. Venkata, M. Kumar, S.-H. Hong, H.-D. Kim, Fabrication of silicon nitride nanoceramics and their tribological properties, Journal of the American Ceramic Society 93 (5) (2010) 1461–1466.
[26] K.J.D. MacKenzie, M.E. Smith, Multinuclear Solid-State NMR of Inorganic Materials, Pergamon Materials Series, 6, Pergamon-Elsevier, Oxford, 2002.
[27] A. Tsuge, K. Nishida, High-strength hot-pressed Si_3N_4 with concurrent Y_2O_3 and Al_2O_3 additions, American Ceramic Society Bulletin 57 (1978) 424–431.
[28] S. Suzuki, T. Nasu, S. Hayama, M. Ozawa, Mechanical and thermal properties of β'-sialon prepared by a slip casting method, Journal of the American Ceramic Society 79 (1996) 1685–1688.
[29] E. Gaffet, F. Bernard, J.-C. Niepce, F. Charlot, C. Gras, G. Le Caer, J.-L. Guichard, P. Delcroix, A. Mocellin, O. Tillement, Some recent developments in mechanical activation and mechanosynthesis, Journal of Materials Chemistry 9 (1999) 305–314.